$$\nu_{\mathrm{mt}} = D_R \frac{[C_R - C_R(x=0)]}{\delta_R} \tag{2.18}$$

$$j = nF\left(\frac{D_{\mathrm{R}}}{\delta_{\mathrm{R}}}[C_R - C_R(x=0)] + \frac{D_{\mathrm{P}}}{\delta_{\mathrm{P}}}[C_P(x=0) - C_P]\right) \tag{2.19}$$

$$\delta = \frac{1.61 \cdot \sqrt[3]{D}\sqrt[6]{\nu}}{\sqrt{\omega}} \tag{2.20}$$

2.2 Modeling at the atomic scale

In science, every model has a certain range of validity. In the case of mechanics, Newton's second law can be applied to a physical system to relate its position and momentum to an external force $\vec{F}$ applied to the system, **Equation 2.21**.[71] Thus, it is possible to define the status of a physical system from the forces applied, predicting its evolution over time.[71] However, the Newton's model of classical mechanics fails when it comes to predict the status of a physical system in the atomic scale, such as a molecule, an atom or one of its constituents (proton, neutron, electron, etc.).

$$\vec{F} = m \cdot \vec{a} \tag{2.21}$$

2.2.1 Schrödinger equation

A revolutionary theory, quantum mechanics,[72] was introduced at the beginning of the 20th century. Seeking to solve the experimental and theoretical evidences of the wave-particles dualism, such as the scattering of X-rays (M. Von Laue,[73] A. H. Compton[74]) and the photoelectric effect (A. Einstein[75]), the Austrian physicist Erwin Schrödinger proposed to describe the status of a physical system by mean of wave functions.[76] According to this formalism, the time-independent Schrödinger equation is an eigenvalues equation, **Equation 2.22**, where $\hat{H}$ is the Hamiltonian operator and Ψ is the state vector of the quantum systems. The Ψ_n eigenstates of the Hamiltonian are the solutions of the previous equation and have n associated eigenvalues E_n, which are real numbers. The expansion in term of the positions eigenvector of the state vector is the position-space wave function of the system, **Equation 2.23**.

$$\begin{aligned} \hat{H}\,|\Psi\rangle &= E\,|\Psi\rangle \\ \hat{H}\Psi_n &= E_n\Psi_n \end{aligned} \tag{2.22}$$

$$\Psi(\vec{r}) = \langle \vec{r}|\Psi\rangle \tag{2.23}$$

The definition of the Hamiltonian depends on the system. In chemical systems such as molecules and atoms, atomic nuclei are much heavier than electrons, since the masses of proton and neutron, the constituents of atomic nuclei, are around 1800 times the mass of an electron. Therefore, electrons' response to external excitation is faster, whereas the nuclear motion is slower due to their higher mass. Following these considerations, the Born-Oppenheimer approximation allows to decouple the contributions of nuclei and electrons to calculate the ground state of the system.[77] Thus, the Hamiltonian, **Equation 2.22**, of a non-relativistic system with multiple nuclei and N electrons can be expressed as **Equation 2.24**. The ground state energy E of the electrons depends on their kinetic energy K, the potential V generated by the "fixed" nuclei and the interaction U between electrons. The all-electron wave function is here represented as **Equation 2.25**. For a simple chemical system such as a CO_2 molecule, the all-electron wave function is a 66-dimensional function (22 electrons with 3 spatial coordinates each) so the analytical solution of **Equation 2.24** for molecular systems is not possible.

$$\left[\underbrace{-\frac{\hbar^2}{2m_\mathrm{e}}\sum_{i=1}^{N}\nabla_i^2}_{\hat{K}}+\underbrace{\sum_{i=1}^{N}V(\vec{r}_i)}_{\hat{V}}+\underbrace{\sum_{i=1}^{N}\sum_{j<1}U(\vec{r}_i,\vec{r}_j)}_{\hat{U}}\right]\Psi=E\Psi \tag{2.24}$$

$$\langle\vec{r}|\Psi\rangle=\Psi(\vec{r}_1,...,\vec{r}_N) \tag{2.25}$$

A further approximation allows to decouple the all-electron wave function as a product of single-electron wave function, where **Equation 2.26** is defined as the Hartree product. Yet, even under this simplification, **Equation 2.24** cannot be solved for real physical systems due to its many-body problem's nature. Decoupling the all-electron wave function for each of its component, the determination of each single-electron wave function depends on U, the interaction between electrons, **Equation 2.24**, therefore it requires the simultaneous determination of all the other components. The U term is needed for solving Schrödinger equation, but it is defined by the solutions of the equation itself.

$$\Psi(\vec{r}_1,...,\vec{r}_N)=\Psi_1(\vec{r})\Psi_2(\vec{r}),...,\Psi_N(\vec{r}) \tag{2.26}$$

An exact estimation of the all-electron wave function is not of physical interest since it is a mathematical formalism and not a physical observable. Instead, the relevant theoretical variable is the probability for N electrons to be localized in a certain set of coordinates, $(\vec{r}_1,...,\vec{r}_N)$. In fact, electrons'

probability can be related to an experimental observable, the electronic density $n(\vec{r})$, as shown in **Equation 2.27**, where $\hat{n}$ is the density operator, δ the Dirac function, N is the number of electrons in the system, and the second summation accounts for the spin s of each electron i. According to Pauli's exclusion principle, each electronic state can be occupied by two electrons only if they have different spin state since these particles are fermions. Finally, to refer to electronic density, $n(\vec{r}) = n(r_x, r_y, r_z)$, instead of the position wave function, $\Psi(\vec{r}_1, ..., \vec{r}_{3N})$, reduces the complexity of the solution from a 3N-dimensional theoretical function to a 3-dimensional physical observable.

$$\begin{aligned} n(\vec{r}) &= \langle \Psi | \, \hat{n}(\vec{r}) \, | \Psi \rangle \\ \hat{n}(\vec{r}) &= \sum_{i=1}^{N} \sum_{s_i} \delta(\vec{r} - \vec{r}_i) \end{aligned} \tag{2.27}$$

2.2.2 Hohenberg-Kohn theorems

In 1964 Hohenberg and Kohn introduced the concept of a universal functional F of the electronic density $n(\vec{r})$,[78] thus they established the basis for the Density Functional Theory (DFT) formalism. By demonstrating two basic properties of this functional, they provided basic concepts toward a solution of the all-electron Schrödinger equation, **Equation 2.24**.

Theorem 1 *The external potential $V(\vec{r})$ is a unique functional of the electronic density: $V(\vec{r}) = F[n(\vec{r})]$. As a consequence, the full many-body ground state is a unique functional of $n(\vec{r})$ since the external potential defines the Hamiltonian of the system.*

Theorem 2 *The electronic density which minimizes the energy of $F[n(\vec{r})]$ corresponds to the electronic density of the ground state resulting from the solution of the many-body Schrödinger equation.*

Thus, it is possible to determine the ground-state energy of a physical system from its ground-state electronic density (3-D function) instead of the all-electron position wave function ($3N$-D function). Moreover, the ground-state electronic density of the physical system is the one that minimizes the energy of the functional. Through a suitable definition of this unique functional, $n(\vec{r})$ can be estimated by solving the many-body Schrödinger equation. By iteration, it is then possible to determine the ground-state electronic density and consequently the ground-state energy of the system.

2.2.3 Kohn-Sham equations

To define this unique functional, it is convenient to decouple the N-electron Schrödinger equation into N single-electron Schrödinger equations. Thus,

the space wave function now reads as a product of the wave function for each electron, **Equation 2.26**. Hence, the resulting Schrödinger equations for each i single-electron wave function reads as **Equations 2.28**, the so-called Kohn-Sham equations.[79] K and V_{N} account respectively for the kinetic energy of the single electron and the potential resulting from the electronic interaction with the atomic nuclei. Both terms follow from **Equation 2.24**.

$$\left[\underbrace{-\frac{\hbar^2}{2m_{\mathrm{e}}}\nabla_i^2}_{\hat{K}} + \underbrace{V_{\mathrm{N}}(\vec{r})}_{\hat{V}_{\mathrm{N}}(\vec{r})} + \underbrace{e^2\int\frac{n(\vec{r}')}{|\vec{r}-\vec{r}'|}d^3\vec{r}'}_{\hat{V}_{\mathrm{H}}(\vec{r})} + \underbrace{\frac{\delta E_{\mathrm{XC}}}{\delta n(\vec{r})}}_{\hat{V}_{\mathrm{XC}}(\vec{r})}\right]\Psi_i(\vec{r}) = E_i\Psi_i(\vec{r}) \quad (2.28)$$

V_{H}, the Hartree potential, **Equation 2.29**, describes the repulsion between the single electron considered and all the other electrons, represented by $n(\vec{r})$. Since each specific electron contributes twice, both as a single-electron and in the electronic density term, the Hartree potential is affected by a non-physical self-interaction effect. Correction to the self-interaction effect as well as contributions by exchange and correlation are included in the last term, the exchange-correlation potential, which is defined for consistency as a functional derivative, **Equation 2.30**. E_{XC} is the only unknown variable in **Equations 2.30** and it can be estimated via different approximations which are discussed in the following section.

$$V_{\mathrm{H}} = e^2\int\frac{n(\vec{r}')}{|\vec{r}-\vec{r}'|}d^3\vec{r}' \quad (2.29)$$

$$V_{\mathrm{XC}} = \frac{\delta E_{\mathrm{XC}}}{\delta n(\vec{r})} \quad (2.30)$$

Given a convenient approximation of the exchange-correlation term, the ground-state energy for a specific system can be calculated solving self-consistently the Kohn-Sham equations,[79] **Equations 2.28**.

1. An initial electron density $n_0(\vec{r})$ is defined.

2. Kohn-Sham equations are solved and the single-electron wave functions $\Psi_{i,0}(\vec{r})$ are determined.

3. A new electronic density $n_1(\vec{r})$ is calculated applying the density operator $\hat{n}(r)$ (**Equation 2.27**) to the single-electron wave functions, **Equation 2.31**.

$$n_1(\vec{r}) = 2\sum_i \Psi_{i,0}^*(\vec{r})\Psi_{i,0}(\vec{r}) \quad (2.31)$$

4. $n_1(\vec{r})$ and $n_0(\vec{r})$ are compared. If they fall within the same tolerance range, then $n_1(\vec{r})$ is defined as the ground-state electronic density and the ground-state energy of the system is computed. Otherwise, $\Psi_{i,1}(\vec{r})$ are calculated and the cycle is repeated from step 3.

Exchange-correlation functionals

According to Pauli's exclusion principle, a specific electronic state can contain two electrons only if they have opposite spin. Therefore, electrons with the same spin must be spatially separated and this leads to a reduction of the Coulomb energy of the system,[80] called exchange energy. Additionally, since the Hartree-Fock approach approximates the all-electron wave function into several single-electron wave function, the energy of the single-electron system needs to be corrected by a factor, named correlation energy. Both exchange and correlation energies are included in the exchange-correlation energy, **Equation 2.30**. This term has to be approximated to allow the solution of the Kohn-Sham equations. Several approximations are possible and their hierarchy in term of accuracy has been defined by John Perdew as "the Jacobs ladder of DFT",[72,81] **Figure 2.5**.

Local-Density Approximation The simplest approximation is the Local-Density Approximation (LDA), introduced by Kohn and Sham in 1965.[79] The exchange-correlation energy of an electronic system is here derived assuming that the exchange-correlation energy per electron at coordinates $\vec{r}$, $\epsilon_{\mathrm{XC}}(\vec{r})$, is the same as in a homogeneous electron gas with the same local electronic density, $\epsilon_{\mathrm{XC}}^{\mathrm{homo}}(\vec{r})$ **Equation 2.32**. The exchange-correlation energy function is treated as a local phenomenon and it is calculated by stochastic methods (Ref.[82]) for high-density electron gases and then interpolated for intermediate and low-density electron gases. Therefore, the LDA approximation guarantees reliable results for bulk solid or any other material with almost constant valence electron density. For atoms, molecules, and other interesting systems the electron density varies locally, thus more complete approaches are needed, since this approximation overestimates bond energies, with error bars of around 2 eV.[83]

$$\begin{aligned} E_{\mathrm{XC,LDA}}[n(\vec{r})] &= \int n(\vec{r})\epsilon_{\mathrm{XC}}^{\mathrm{homo}}(\vec{r})d^3\vec{r'} \\ \frac{\delta E_{\mathrm{XC,LDA}}}{\delta n(\vec{r})} &= \frac{\partial \epsilon_{\mathrm{XC}}^{\mathrm{homo}}(\vec{r})n(\vec{r})}{\partial n(\vec{r})} \end{aligned} \tag{2.32}$$

Generalized Gradient Approximation The Generalized Gradient Approximation (GGA) includes the spatial variation of the electronic density

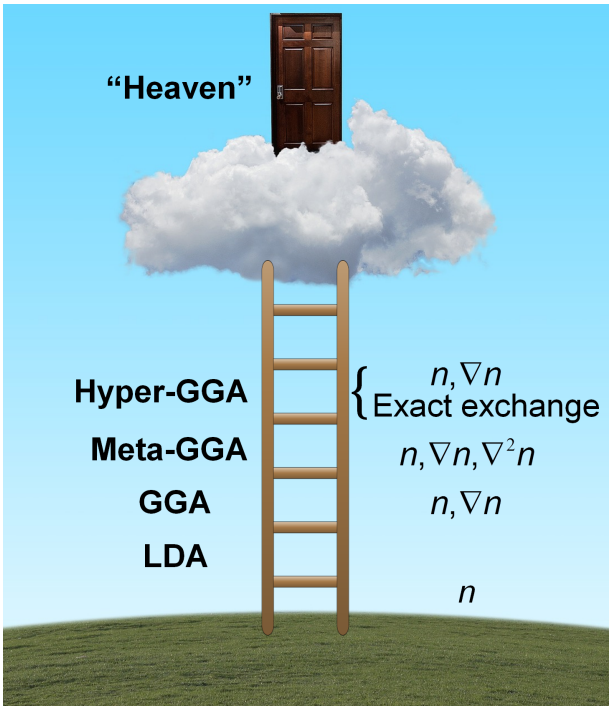

Figure 2.5: Perdew classification of DFT functional from the simplest approximation, the Local-Density approximation, to hybrid functionals which explicitly account for exchange. Adapted from Ref.[72].

of a physical system by accounting for both the local electron density $n(\vec{r})$ and its gradient $\nabla n(\vec{r})$, **Equation 2.33**. In this way, this approximation accounts as well for systems which have slowly varying electronic densities. As LDA, nonempirical GGA functionals satisfy the uniform density limit: at the limit of uniform density, the exchange-correlation energy reproduces the uniform electron gas energy at that electronic density. Among nonempirical GGA functionals, Perdew-Wang 91 (PW91)[84] and Perdew-Burke-Ernzerhof (PBE)[85] functional are widely employed. Since GGA functionals do not account for the London dispersion forces, their application leads to an underestimation of physisorption of molecules on metal surfaces.[86,87] Many corrections such as the Grimme's empirical methods,[88–91] vdw-DF,[92] vdw-DF2,[93] and the Tkatchenko-Scheffler method[94] are usually included to improve the accuracy of the calculation of adsorption energies.

$$E_{\mathrm{XC,GGA}}[n(\vec{r})] = \int n(\vec{r})\epsilon_{\mathrm{XC}}[n(\vec{r}), \nabla n(\vec{r})]d^3\vec{r} \tag{2.33}$$

Meta-GGA functionals Meta-GGA functionals extend the GGA approach by including second order derivatives of the electronic density of a physical systems,[95] **Equation 2.34**.

$$E_{\mathrm{XC,GGA}}[n(\vec{r})] = \int n(\vec{r})\epsilon_{\mathrm{XC}}[n(\vec{r}), \nabla n(\vec{r}), \nabla^2 n(\vec{r})]d^3\vec{r'} \tag{2.34}$$

Hybrid-GGA functionals Hybrid-GGA functionals describe exchange-correlation energy by including contributions from both exact exchange and GGA exchange functionals. For instance, B3LYP[96–98] functional is defined as **Equation 2.35**, where $E_{\mathrm{C}}^{\mathrm{LDA}}$ is the LDA contribution,[99] $E_{\mathrm{X}}^{\mathrm{GGA}}$ is the Becke 88 exchange functional,[100] $E_{\mathrm{C}}^{\mathrm{GGA}}$ is the Lee-Yang-Parr correlation functional,[96] α_1, α_2, α_3 are numerical parameters, and E^{exchange} is the exact exchange energy calculated over the occupied orbitals ϕ_i by **Equation 2.36**. Hybrid functionals are convenient for DFT calculations based on localized basis sets, whilst they increase the complexity of solving Kohn-Shan equations in a plane-wave basis set. Therefore, these functionals are hardly employed for simulations of supercells which require periodic boundary conditions. Furthermore, the explicit calculation of the exact exchange term prevents hybrid functionals from satisfying the uniform density limit, which make them unsuitable for metals. Hence, functionals developed under the Generalized Gradient Approximation, such as the Perdew-Burke-Ernzerhof (PBE),[85] are used for investigating metallic surfaces.

$$\begin{aligned} E_{\mathrm{XC}}^{\mathrm{B3LYP}} =& E_{\mathrm{XC}}^{\mathrm{LDA}} + \alpha_1(E^{\mathrm{exchange}} - E_{\mathrm{X}}^{\mathrm{LDA}}) + \alpha_2(E_{\mathrm{X}}^{\mathrm{GGA}} - E_{\mathrm{X}}^{\mathrm{LDA}}) + \\ & \alpha_3(E_{\mathrm{C}}^{\mathrm{GGA}} - E_{\mathrm{C}}^{\mathrm{LDA}}) \end{aligned} \tag{2.35}$$

$$E^{\mathrm{exchange}}(\vec{r}) = \frac{1}{2n(\vec{r})} \int d^3\vec{r'} \frac{|\sum_i \phi_i^*(\vec{r'})\phi_i(\vec{r})|}{|\vec{r} - \vec{r'}|} \tag{2.36}$$

Periodic systems

Heterogeneous catalysis involves catalysts with a different phase from products and reactants. For electrochemical CO_2 reactions, heterogeneous catalysts are usually solid materials. In this study, I focused on copper, a crystal which is solid at standard conditions. A crystal is defined as a three-dimensional periodic structure of identical building blocks of atoms.[101] The identical building block is defined basis and the set of points which describes the periodicity is called Bravais lattice. The lattice is usually composed by three linearly independent translation vectors, $\vec{a}_1$, $\vec{a}_2$, and $\vec{a}_3$, whose directions determine the crystal axes as well. If the periodicity of each basis satisfies **Equation 2.37** for every arbitrary integers n_1, n_2, and n_3, these lattice vectors are named primitive translation vectors. The geometric

block defined by the primitives axes $\vec{a_1}$, $\vec{a_2}$, and $\vec{a_3}$ is called primitive cell or Wigner-Seitz cell. It is the basis or building block which contains the fewer atoms possible. Overall, the periodicity of crystals is described by 14 different lattice types. In the case of copper, at room temperature its periodicity accounts for a face-centered cubic lattice (fcc).

$$\vec{R} = n_1\vec{a_1} + n_2\vec{a_2} + n_3\vec{a_3} \tag{2.37}$$

From the Bravais lattice it is useful to derive the reciprocal lattice, constructed by the reciprocal cell vectors $\vec{b_1}$, $\vec{b_2}$, and $\vec{b_3}$ defined as **Equations 2.38**. The reciprocal lattice relative to the primitive cell is named Brillouin zone. The three primitive vectors of the reciprocal lattice combine into the reciprocal lattice vector $\vec{G}$, **Equation 2.39**, with u_1, u_2 and u_3 as integer numbers. Whilst the lattice vectors $\vec{a_j}$ are measured in Å, the reciprocal lattice vectors have $Å^{-1}$ as unit.

$$\begin{aligned}
\vec{b_1} &= 2\pi\frac{\vec{a_2}\times\vec{a_3}}{\vec{a_1}\cdot\vec{a_2}\times\vec{a_3}} \\
\vec{b_2} &= 2\pi\frac{\vec{a_3}\times\vec{a_1}}{\vec{a_1}\cdot\vec{a_2}\times\vec{a_3}} \\
\vec{b_3} &= 2\pi\frac{\vec{a_1}\times\vec{a_2}}{\vec{a_1}\cdot\vec{a_2}\times\vec{a_3}}
\end{aligned} \tag{2.38}$$

$$\vec{G} = v_1\vec{b_1} + v_2\vec{b_2} + v_3\vec{b_3} \tag{2.39}$$

A bulk crystal can be cleaved to produce crystal planes. The orientation of these crystal facets is represented by its Miller indices, which are defined from the lattice vectors according to a specific methodology. The intercepts (i_1,i_2,i_3) between the crystal axes and the crystal plane are defined in term of $\vec{a}_1$, $\vec{a}_2$, $\vec{a}_3$. The surface orientation of a given facet is then determined by the reciprocals of the intercepts (${i_1}^{-1}$,${i_2}^{-1}$,i_3^{-1}). If a plane does not intercept an axis, then the corresponding index is 0. In case of a negative intercept $-i$, then the Miller index is written as $\bar{h} = i^{-1}$. Planes which are equivalent by symmetry as denoted by curly brackets, as for instance $\{h_1h_2h_3\}$. For fcc metals as copper the most stable orientation is the (111) cut.

Bloch's Theorem

The single-electron Schrödinger equation can be solved numerically for different basis sets. Basis sets composed of atomic orbitals are usually employed in quantum chemistry for simulating the properties of isolated molecules and chemical compounds. For solid state systems, a better choice is the plane-waves basis set, which employs the periodicity of the simulated

structure to significantly decrease the computing time. This formalism is based on the Bloch's theorem.[102]

The potential energy of an electron in a periodic system is invariant under a crystal lattice translation $\vec{R}$, which is a linear combination of the lattice vectors $\vec{a}_1$, $\vec{a}_2$, and $\vec{a}_3$, **Equation 2.40**. Thus, Bloch's theorem states that the eigenstates of the single-electron wave function, **Equation 2.28**, can be written as a product of a cell periodic part, **Equation 2.41**, and a wave-like part dependent on the the wave vectors $\vec{k}$, called k-points, **Equation 2.42**. For each wave vector $\vec{k}$, the exact definition of the eigenstate Ψ_j would require a infinite summation over the plane waves. Yet, since contributions of high kinetic energies plane waves are minor, we can limit their number by setting a kinetic energy cutoff. Additionally, the single-electron wave function is composed by the eigenstates calculated for each k point. Thus, the k-points sampling defines the integration grid in the first Brillouin zone and a high k-points density leads to an increase of accuracy at the expenses of computational time. Nevertheless, since electronic wave function for similar k-points are almost identical, their sampling can be reduced, following as well considerations on symmetry.[103]

$$U(\vec{r}) = U(\vec{r} + \vec{T}) \tag{2.40}$$

$$u_j(\vec{r}) = u_j(\vec{r} + \vec{T}) = \sum_{\vec{G}} C(\vec{k} + \vec{G}) e^{+i\vec{G}\cdot\vec{r}} \tag{2.41}$$

$$\Psi_j(\vec{r}) = u_j(\vec{r}) e^{i\vec{k}\cdot\vec{r}} \tag{2.42}$$

Pseudopotentials

Bloch's theorem allows for a reduction of simulation time due to a proper choice of k-points sampling and energy cutoff. However, a plane-waves basis expansion over both core and valence electrons would dramatically increase the computational burden, due to the high numbers of plane waves required to account for the rapid oscillations of the valence electrons wave functions in the core region. Usually, valence electrons determine the chemical properties of physical systems more significantly than core electrons, since core electrons are strongly bound to the nuclei and interact with the surrounding to a lower extent. Therefore, the pseudopotential approximation allows to replace the core electrons and the strong ionic potential between nucleus and core electrons with a weaker pseudopotential based on a set of pseudo wave functions, **Figure 2.6**. Only valence electrons are explicitly assessed for the numerical solution of Kohn-Sham Equations, **Equations 2.28**. From a cut-off radius r_c all electron and pseudopotential wave functions overlap. Key

properties of the so-defined pseudopotentials are their transferability and softness. To have transferable pseudopotentials means that they reproduce inner electrons properties irrespectively from the atomic valence electrons. To have soft pseudopotentials implies that the plane-waves expansion of the valence electrons wave functions must be limited to the lowest energy cutoff possible to decrease simulation time. A high cutoff radius implies an increase of pseudopotentials softness at the detriment of transferability, whilst the opposite holds true as well. The most employed pseudopotentials are the Vanderbilt ultrasoft (US-PP)[104] and the Projector-Augmented Wave pseudopotentials (PAW).[105] For the entire study, I employed PAW pseudopotentials since they perform better for transition metals.[106]

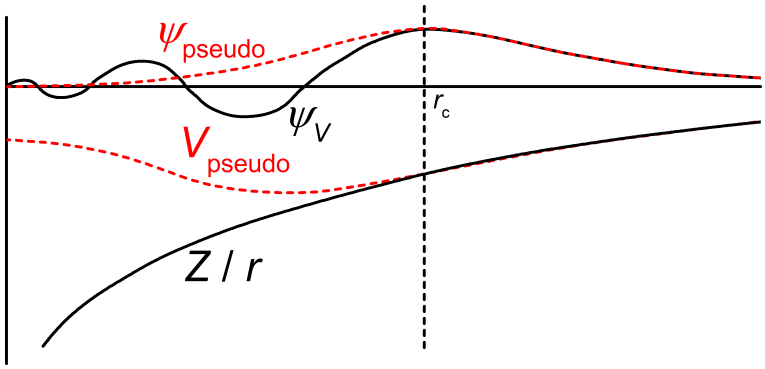

Figure 2.6: All electron (black line) and pseudoelectron (red line) wave functions and corresponding potentials. Pseudoelectron wave functions and potentials overlap with all electron values from the cutoff radius r_c. Adapted from Ref.[80].

2.3 The Computational Hydrogen Electrode

DFT methodologies based on periodic boundaries conditions cannot account for charged cells. Thus, basic electrochemical phenomena, such as electron transfer, pH, and electric potential, are hard to model. A simple model which has been applied to electrocatalysis is the Computational Hydrogen Electrode (CHE).[65] This methodology was proposed for the Oxygen Reduction Reaction (ORR),[65] however it was soon extended to additional chemical reactions, akin electrochemical CO_2 reduction.[9] It allows to calculate intermediate adsorption energy including electron transfer, electric potential, and pH. This approach is based on the following hypotheses.

1. Taking as reference potential the Standard Hydrogen Electrode (SHE), the chemical potential for the reaction $H^+ + e^-$ can be related

to the Gibbs free energy of $\frac{1}{2}H_2$. Therefore, at standard conditions (298 K, 1 bar of gas phase H_2), **Equation 2.43** is valid.

$$G_{H^+} = \frac{1}{2} G_{H_2,\mathrm{DFT}} \tag{2.43}$$

2. The effect of the electric potential is included adding to a thermodynamic state the energy of each transferred electron, ne^-U, where U is the applied potential. **Figure 2.7** shows a practical example for CO_2 reduction to CO.

3. The effect on the intermediates of the electrostatic field caused by the electrical double layer is neglected since calculated within DFT intrinsic error (0.01 eV). In case of intermediates with large electric dipole moments $\vec{\mu}$, the stabilization is estimated as $\mu_z \cdot E_z$.[65,107]

4. Proton Gibbs free energy is corrected for pH > 0 by the entropy related to H^+ concentration, **Equation 2.44**.

$$G(\mathrm{pH}) = -k_B T \ln H^+ = k_B T \cdot \ln(10) \cdot \mathrm{pH} \tag{2.44}$$

5. Solvation contribution must be included either through explicit insertion of water molecules in the simulation box[65] or implicit model based on solvent dielectric permittivity.[108,109]

6. The DFT energies for the reaction intermediates must be corrected by their zero point energies and the influence of entropy at the reaction temperature T, **Equation 2.45**.

$$\Delta G = \Delta E_{\mathrm{DFT}} + \Delta E_{\mathrm{ZPE}} - T\Delta S \tag{2.45}$$

The CHE model assumes for simplicity every electron transfer as a proton-coupled electron transfer. Therefore, its application to decoupled proton-electron transfers, such as CO_2 adsorption, has intrinsic limitations.[18] An alternative model derived from Marcus theory (Ref.[110]) has been proposed to account for the transition between sequential and concerted proton-electron transfer.[111–113]

2.4 Molecular Dynamics

As explained in **Section 2.2**, the application of Density Functional Theory is limited to steady states systems since this theory is based on the solution of the time-independent Schrödinger equation. However, to assess interesting phenomena such as reconstruction of complex materials or *Operando*

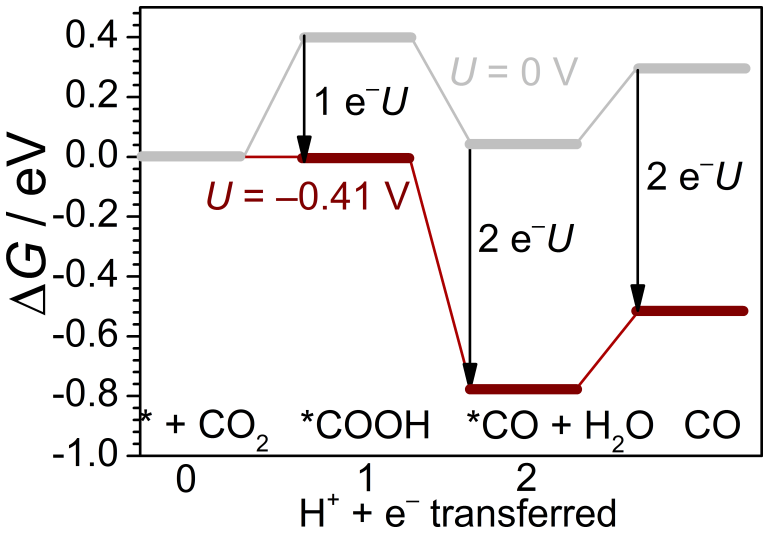

Figure 2.7: Application of the CHE approach to the modeling of CO_2 reduction toward CO. For every proton-coupled electron transfer, the Gibbs free energy of the reaction intermediate is corrected by a $e^{-}U$ factor. Adapted from Ref.[9].

catalysts the atomic motions need to be simulated. Thus, another useful tool for a theoretical electrochemist is the formalism of Ab Initio Molecular Dynamics.[72,114]

2.4.1 Classical Molecular Dynamics

Microcanonical ensemble

In classical mechanics, the status of a system with N components having mass m_i in a volume V, is defined by their $3N$ coordinates, $\{r_1, ...r_{3N}\}$, and the components of their velocities, $\{v_1, ..., v_{3N}\}$. Due to the law of conservation of energy, the overall energy of the system E does not change over time, **Equation 2.46**. Thus, E is given by the sum of kinetic and potential energy, respectively K and U. In statistical dynamics this system of components is called microcanonical ensemble, since the number of components N, its volume V, and the overall energy is constant. Recalling the Newton's law of motion, **Equation 2.21**, and since the force applied to the system is the negative gradient of the total potential energy, **Equation 2.47**, the time evolution of all the components is described by the solution of a system of $6N$ first-order differential equations, **Equation 2.48**. Given the number of atoms contained in a physical system, these equations cannot be solved analytically for a realistic material. However, applying Taylor expansion,

the time evolution of an atom can be derived by its previous position and the resulting force through the Verlet algorithm, **Equation 2.49**, if the time step Δt is small. The velocities of the atoms of a real system depend on its temperature T and follow Maxwell-Boltzmann distribution. According to this distribution, the average kinetic energy of each degree of freedom scales with its temperature, **Equation 2.50**, therefore the velocities of the atoms correlate with the kinetic energy of the system and consequently with its temperature.

$$E = K - U = \frac{1}{2}\sum_{i=1}^{3N} m_i v_i^2 - U(r_1, ..., r_{3N}) \tag{2.46}$$

$$\vec{F_i} = m_i \cdot \vec{a_i} = m_i \frac{\mathrm{d}\vec{v_i}}{\mathrm{d}t} = -\frac{\partial U}{\partial \vec{r_i}} \tag{2.47}$$

$$\begin{aligned} \frac{\mathrm{d}r_i}{\mathrm{d}t} &= v_i \\ \frac{\mathrm{d}v_i}{\mathrm{d}t} &= -\frac{1}{m_i}\frac{\partial U(r_1, ..., r_{3N})}{\partial r_i} \end{aligned} \tag{2.48}$$

$$\vec{r_i}(t + \Delta t) \cong 2\vec{r_i}(t) - \vec{r_i}(t - \Delta t) + \frac{\vec{F_i}}{m_i}\Delta t^2 \tag{2.49}$$

$$\frac{1}{2}m\overline{v^2} = \frac{k_\mathrm{B}T}{2} \tag{2.50}$$

Canonical ensemble

A real system exchanges heat with the environment, thus experimental conditions are better described by a canonical ensemble, which is a system where the number of atoms N, the volume V, and the temperature T are constant. To adapt the equations of motion of a microcanonical ensemble to a canonical ensemble, Nosé introduced a fictitious heat reservoir through an additional degree of freedom s.[115] Hence, the Lagrangian of the system, a mathematical function which describes its dynamics, reads as **Equation 2.51**. The parameter g, equal to the overall number of the degrees of freedom, is chosen to satisfy the canonical distribution at the equilibrium. Q is a factor which behaves as the effective mass of s and T is the temperature set for the system. If $s(t) = 1$, **Equation 2.51** simplifies to **Equation 2.52**, which is the Lagrangian of a microcanonical ensemble. The Lagrangian formalism allows to determine the equations of motion of every single constituent of the system as **Equations 2.53** for each of the $3N$ degrees of freedom.

$$L = K - U = \frac{1}{2}\sum_{i=1}^{3N} m_i v_i^2 s^2 - U(r_1, ..., r_{3N}) + \frac{Q}{2}\left(\frac{\partial s}{\partial t}\right)^2 - g k_{\mathrm{B}} T \ln s \quad (2.51)$$

$$L = K - U = \frac{1}{2}\sum_{i=1}^{3N} m_i v_i^2 - U(r_1, ..., r_{3N}) \quad (2.52)$$

$$\frac{\mathrm{d}}{\mathrm{d}t}\left(\frac{\partial L}{\partial v_i}\right) = \frac{\partial L}{\partial r_i} \quad (2.53)$$

After the pioneering work of Nosé, Hoover derived the equations of motion for the extended Lagrangian as **Equations 2.54**,.[116] The parameter ζ acts as a feedback term which increases or decreases the velocities of the atom depending on its sign and it is controlled by the instantaneous temperature of the atoms in the system, T_{inst}. According to Maxwell-Boltzmann distribution, each degree of freedom accounts for a kinetic energy of $\frac{k_B T}{2}$, **Equation 2.50**, therefore the feedback loop is explicit, **Equation 2.55**. If the temperature of the system, T_{inst} is beyond the chosen value T, ζ increases, thus lessening the velocities of each constituent. Otherwise, if the instantaneous temperature is low, ζ is diminished, leading to an increase of the kinetic energy of the system. The Q, defined before as the mass of s, controls the speed of the feedback loop. **Equations 2.54** can be solved numerically through an extension of the Verlet algorithm, **Equation 2.49**. Therefore, this derivation, so-called Nosé-Hoover thermostat,[117] allows to study the time evolution of a system at a constant temperature T. From position $\vec{r}_i$, friction ζ, and forces $\vec{F}_i$ at time t, it is possible to calculate the positions at time $t + \Delta t$, **Equation 2.56**. Since the forces applied to the system need to be determined at every time step, bigger is the investigated system, larger is the computational cost of a Molecular Dynamics simulation. Additionally, the Verlet algorithm is valid only for small times steps, due to its derivation through a Taylor series of Δt. By definition, a Molecular Dynamics simulation should describe fast motions as atomic vibrational frequencies, thus a suitable time step should be set in the order of the fs.

$$\begin{aligned}
\frac{\mathrm{d}r_i}{\mathrm{d}t} &= v_i \\
\frac{\mathrm{d}v_i}{\mathrm{d}t} &= -\frac{1}{m_i}\frac{\partial U(r_1, ..., r_{3N})}{\partial r_i} - \zeta v_i \\
\frac{\mathrm{d}\zeta}{\mathrm{d}t} &= \frac{1}{Q}\left[\sum_{i=1}^{3N} m_i v_i^2 - 3N k_{\mathrm{B}} T\right] \\
\frac{\mathrm{d}\ln s}{\mathrm{d}t} &= \zeta
\end{aligned} \quad (2.54)$$

$$\frac{\mathrm{d}\zeta}{\mathrm{d}t} = \frac{1}{Q}\left[\sum_{i=1}^{3N} m_i v_i^2 - 3Nk_\mathrm{B}T\right] = \frac{3Nk_\mathrm{B}}{Q}[T_\mathrm{inst} - T] \tag{2.55}$$

$$\vec{r_i}(t+\Delta t) \cong 2\vec{r_i}(t) - \vec{r_i}(t-\Delta t) + (\frac{\vec{F_i}}{m_i} - \zeta\vec{v_i})\Delta t^2 \tag{2.56}$$

2.4.2 Ab Initio Molecular Dynamics

Classical molecular dynamics allows to describe the dynamics of N atoms provided the estimation of their potential energy as a function of their spatial coordinates, $U(r_1, ..., r_{3N})$. As demonstrated in **Section 2.2**, Density Functional Theory can be applied for this purpose. The Lagrangian for a molecular system can then be expressed as **Equation 2.57**. $\Psi(r_1, ..., r_{3N})$ are the Kohn-Sham one-electron wave functions which represent the electronic ground state for the $3N$ degrees of freedom of the complex. This Lagrangian is valid for a microcanonical ensemble, thus at constant N, V and E.

$$L = K - U = \frac{1}{2}\sum_{i=1}^{3N} m_i v_i^2 - E[\Psi(r_1, ..., r_{3N})] \tag{2.57}$$

The workflow for an Ab Initio Molecular Dynamics starts with the determination of the ground-state energy from the initial coordinates of the atoms of system. Then Classical Molecular Dynamics (**Section 2.4.1**) is applied and the nuclear positions of the atoms are updated depending on the applied forces. Finally, the ground-state energy of the updated configurations is calculated through DFT and the resulting forces are determined from the potential energy. If the Kohn-Shan equations are explicitly solved, this methodology is described as Born-Oppenheimer Molecular Dynamics (BOMD). The determination of the ground-state energy of the updated configuration is expedited using the electronic properties of the system for the previous molecular dynamics steps, thus making BOMD simulations computationally viable. An alternative methodology by Car and Parinello, the Car-Parinello Molecular Dynamics (CPMD),[118] is based on the parallel calculation of the dynamics of the atomic nuclei and the ground-state energy. The equations of motions for both the nuclear and electronic degrees of freedom are described by a generalized Lagrangian, which includes the electronic degrees of freedom as fictitious dynamical variables. However, this approximation makes CPMD less accurate than BOMD.

2.5 General computational details

Throughout the whole thesis, I carried out Density Functional Theory simulations of surfaces, adsorbates, and reference molecules in gas phase following some general guidelines.

I employed the Vienna Ab Initio Simulation Package (VASP)[119,120] and used the PBE as the density functional.[85] Inner electrons were always represented by PAW pseudopotentials[105,106] and a kinetic energy cutoff of 450 eV was chosen for the expansion as plane waves of the monoelectronic states for the valence electrons. I sampled the Brillouin zone with a Γ-centered k-points mesh from the Monkhorst-Pack method,[103] large enough to provide a reciprocal grid size smaller than 0.03 $Å^{-1}$. In the case of surfaces, I followed the supercell approximation, thus building a 2D-periodic surface of several atomic layers with an upper vacuum thickness large enough to avoid interactions in the z-directions. As for the molecules, they were simulated in box of 10-20 Å size to circumvent spurious interactions given by periodic boundary conditions. I included dispersion through the DFT-D2 method[88,121] with the C_6 coefficients for the metals reparametrized as in Ref.[89] to assess the adsorption of reaction intermediates. I included solvation effects through implicit models based on the VASP-MGCM framework (Refs.[108, 109]) and the VASPsol code (Refs.[122, 123]). When I employed asymmetric simulation cells, I applied a dipole correction to remove artifacts generated by asymmetry.[124] Upon estimation of solvent effects, dipole correction was deactivated.

If specific computational parameters were needed, I highlighted the different choice of set chapter by chapter.

[62] Dattila, F.; García-Muelas, R.; López, N. Active and selective ensembles in oxide-derived copper catalysts for CO_2 reduction, *ACS Energy Lett.* **2020,** *5,* 3176–3184.

[63] Gupta, N.; Gattrell, M.; MacDougall, B. Calculation for the cathode surface concentrations in the electrochemical reduction of CO_2 in $KHCO_3$ solutions, *J. Appl. Electrochem.* **2006,** *36,* 161–172.

[64] Ringe, S.; Clark, E. L.; Resasco, J.; Walton, A.; Seger, B.; Bell, A. T.; Chan, K. Understanding cation effects in electrochemical CO_2 reduction, *Energy Environ. Sci.* **2019,** *12,* 3001–3014.

[65] Nørskov, J. K.; Rossmeisl, J.; Logadottir, A.; Lindqvist, L.; Kitchin, J. R.; Bligaard, T.; Jónsson, H. Origin of the overpotential for oxygen reduction at a fuel-cell cathode, *J. Phys. Chem. B* **2004,** *108,* 17886–17892.

[66] Bard, A. J.; Faulkner, L. R. *Electrochemical methods: Fundamentals and applications,* 2^{nd} *edition;* John Wiley & Sons, Inc.: 2001.

[67] Shinagawa, T.; Garcia-Esparza, A. T.; Takanabe, K. Insight on Tafel slopes from a microkinetic analysis of aqueous electrocatalysis for energy conversion, *Sci. Rep.* **2015,** *5,* 13801.

[68] Mills, J. N.; McCrum, I. T.; Janik, M. J. Alkali cation specific adsorption onto fcc(111) transition metal electrodes, *Phys. Chem. Chem. Phys.* **2014,** *16,* 13699–13707.

[69] Rudnev, A. V.; Kiran, K.; Broekmann, P. Specific cation adsorption: Exploring synergistic effects on CO_2 electroreduction in ionic liquids, *ChemElectroChem* **2020,** *7,* 1897–1903.

[70] Bagger, A.; Arnarson, L.; Hansen, M. H.; Spohr, E.; Rossmeisl, J. Electrochemical CO reduction: A property of the electrochemical interface, *J. Am. Chem. Soc.* **2019,** *141,* 1506–1514.

[71] Newton, I. *The Principia: Mathematical principles of natural philosophy;* University of California Press: 1999.

[72] Sholl, D.; Steckel, J. A. *Density functional theory: A practical introduction;* John Wiley & Sons: 2009.

[73] von Laue, M. *Concerning the detection of X-ray interferences*, `https://www.nobelprize.org/prizes/physics/1914/laue/lecture/`, 1920 Online; accessed 13 July 2020.

[74] Compton, A. H. *X-rays as a branch of optics*, `https://www.nobelprize.org/prizes/physics/1927/compton/lecture/`, 1927 Online; accessed 13 July 2020.

[75] Einstein, A. Über einen die erzeugung und verwandlung des lichtes betreffenden heuristischen gesichtspunkt, *Ann. Phys.* **1905,** *322,* 132–148.

[76] Schrödinger, E. Quantisierung als eigenwertproblem, *Ann. Phys.* **1926,** *384,* 361–376.

[77] Born, M.; Oppenheimer, R. Zur quantentheorie der molekeln, *Ann. d. Phys.* **1927,** *389,* 457–484.

[78] Hohenberg, P.; Kohn, W. Inhomogeneous electron gas, *Phys. Rev.* **1964,** *136,* B864.

[79] Kohn, W.; Sham, L. J. Self-consistent equations including exchange and correlation effects, *Phys. Rev.* **1965,** *140,* A1133.

[80] Payne, M. C.; Teter, M. P.; Allan, D. C.; Arias, T. A.; Joannopoulos, J. D. Iterative minimization techniques for *ab initio* total-energy calculations: Molecular dynamics and conjugate gradients, *Rev. Mod. Phys.* **1992,** *64,* 1045.

[81] López, N.; Almora-Barrios, N.; Carchini, G.; Błoński, P.; Bellarosa, L.; García-Muelas, R.; Novell-Leruth, G.; García-Mota, M. State-of-the-art and challenges in theoretical simulations of heterogeneous catalysis at the microscopic level, *Catal. Sci. Technol.* **2012,** *2,* 2405–2417.

[82] Ceperley, D. M.; Alder, B. J. Ground state of the electron gas by a stochastic method, *Phys. Rev. Lett.* **1980,** *45,* 566.

[83] Jones, R. O.; Gunnarsson, O. The density functional formalism, its applications and prospects, *Rev. Mod. Phys.* **1989,** *61,* 689.

[84] Perdew, J. P.; Wang, Y. Accurate and simple analytic representation of the electron-gas correlation energy, *Phys. Rev. B* **1992,** *45,* 13244.

[85] Perdew, J. P.; Burke, K.; Ernzerhof, M. Generalized gradient approximation made simple, *Phys. Rev. Lett.* **1996,** *77,* 3865-3868.

[86] Carrasco, J.; Santra, B.; Klimeš, J.; Michaelides, A. To wet or not to wet? Dispersion forces tip the balance for water ice on metals, *Phys. Rev. Lett.* **2011,** *106,* 026101.

[87] Błonski, P.; López, N. On the adsorption of formaldehyde and methanol on a water-covered Pt(111): A DFT-D study, *J. Phys. Chem. C* **2012,** *116,* 15484–15492.

[88] Grimme, S. Semiempirical GGA-type density functional constructed with a long-range dispersion correction, *J. Comput. Chem.* **2006,** *27,* 1787–1799.

[89] Almora-Barrios, N.; Carchini, G.; Błoński, P.; López, N. Costless derivation of dispersion coefficients for metal surfaces, *J. Chem. Theory Comput.* **2014,** *10,* 5002–5009.

[90] Grimme, S. Accurate description of van der Waals complexes by density functional theory including empirical corrections, *J. Comput. Chem.* **2004,** *25,* 1463–1473.

[91] Grimme, S.; Antony, J.; Ehrlich, S.; Krieg, H. A consistent and accurate *ab initio* parametrization of density functional dispersion correction (DFT-D) for the 94 elements H-Pu, *J. Chem. Phys.* **2010,** *132,* 154104.

[92] Dion, M.; Rydberg, H.; Schröder, E.; Langreth, D. C.; Lundqvist, B. I. Van der Waals density functional for general geometries, *Phys. Rev. Lett.* **2004,** *92,* 246401.

[93] Lee, K.; Murray, É. D.; Kong, L.; Lundqvist, B. I.; Langreth, D. C. Higher-accuracy van der Waals density functional, *Phys. Rev. B* **2010,** *82,* 081101.

[94] Tkatchenko, A.; Scheffler, M. Accurate molecular van der Waals interactions from ground-state electron density and free-atom reference data, *Phys. Rev. Lett.* **2009,** *102,* 073005.

[95] Tao, J.; Perdew, J. P.; Staroverov, V. N.; Scuseria, G. E. Climbing the density functional ladder: Nonempirical meta–generalized gradient approximation designed for molecules and solids, *Phys. Rev. Lett.* **2003,** *91,* 146401.

[96] Lee, C.; Yang, W.; Parr, R. G. Development of the Colle-Salvetti correlation-energy formula into a functional of the electron density, *Phys. Rev. B* **1988,** *37,* 785.

[97] Becke, A. D. Density-functional thermochemistry. III. The role of exact exchange, *J. Chem. Phys.* **1993,** *98,* 5648.

[98] Stephens, P. J.; Devlin, F. J.; Chabalowski, C. F.; Frisch, M. J. Ab initio calculation of vibrational absorption and circular dichroism spectra using density functional force fields, *J. Phys. Chem.* **1994,** *98,* 11623–11627.

[99] Vosko, S. H.; Wilk, L.; Nusair, M. Accurate spin-dependent electron liquid correlation energies for local spin density calculations: critical analysis, *Can. J. Phys.* **1980,** *58,* 1200–1211.

[100] Becke, A. D. Density-functional exchange-energy approximation with correct asymptotic behavior, *Phys. Rev. A* **1988,** *38,* 3098.

[101] Kittel, C. *Introduction to solid state physics, 8th edition;* John Wiley & Sons, Inc.: 2005.

[102] Bloch, F. Über die quantenmechanik der elektronen in kristallgittern, *Z. Phys.* **1929,** *52,* 555–600.

[103] Monkhorst, H. J.; Pack, J. D. Special points for Brillouin-zone integrations, *Phys. Rev. B* **1976,** *13,* 5188.

[104] Vanderbilt, D. Soft self-consistent pseudopotentials in a generalized eigenvalue formalism, *Phys. Rev. B* **1990,** *41,* 7892.

[105] Blöchl, P. E. Projector augmented-wave method, *Phys. Rev. B* **1994,** *50,* 17953.

[106] Kresse, G.; Joubert, D. From ultrasoft pseudopotentials to the projector augmented-wave method, *Phys. Rev. B* **1999,** *59,* 1758.

[107] Jiang, K.; Sandberg, R. B.; Akey, A. J.; Liu, X.; Bell, D. C.; Nørskov, J. K.; Chan, K.; Wang, H. Metal ion cycling of Cu foil for selective C–C coupling in electrochemical CO_2 reduction, *Nat. Catal.* **2018,** *1,* 111–119.

[108] Garcia-Ratés, M.; López, N. Multigrid-based methodology for implicit solvation models in periodic DFT, *J. Chem. Theory Comput.* **2016,** *12,* 1331–1341.

[109] Garcia-Ratés, M.; García-Muelas, R.; López, N. Solvation effects on methanol decomposition on Pd(111), Pt(111), and Ru(0001), *J. Phys. Chem. C* **2017,** *121,* 13803–13809.

[110] Marcus, R. A. On the theory of electron-transfer reactions. VI. Unified treatment for homogeneous and electrode reactions, *J. Chem. Phys.* **1965,** *43,* 679–701.

[111] Koper, M. T. M. Theory of the transition from sequential to concerted electrochemical proton-electron transfer, *Phys. Chem. Chem. Phys.* **2013,** *15,* 1399–1407.

[112] Koper, M. T. M. Theory of multiple proton-electron transfer reactions and its implications for electrocatalysis, *Chem. Sci.* **2013,** *4,* 2710–2723.

[113] Göttle, A. J.; Koper, M. T. M. Proton-coupled electron transfer in the electrocatalysis of CO_2 reduction: Prediction of sequential *vs.* concerted pathways using DFT, *Chem. Sci.* **2017,** *8,* 458–465.

[114] Marx, D.; Hutter, J. *Ab initio molecular dynamics: Basic theory and advanced methods;* Cambridge University Press: 2009.

[115] Nosé, S. A unified formulation of the constant temperature molecular dynamics methods, *J. Chem. Phys.* **1984,** *81,* 511–519.

[116] Hoover, W. G. Canonical dynamics: Equilibrium phase-space distributions, *Phys. Rev. A* **1985,** *31,* 1695.

[117] Evans, D. J.; Holian, B. L. The Nose-Hoover thermostat, *J. Chem. Phys.* **1985,** *83,* 4069.

[118] Car, R.; Parinello, M. Unified approach for molecular dynamics and density-functional theory, *Phys. Rev. Lett.* **1985,** *55,* 2471.

[119] Kresse, G.; Furthmüller, J. Efficient iterative schemes for *ab initio* total-energy calculations using a plane-wave basis set, *Phys. Rev. B* **1996,** *54,* 11169.

[120] Kresse, G.; Furthmüller, J. Efficiency of ab-initio total energy calculations for metals and semiconductors using a plane-wave basis set, *Computat. Mater. Sci.* **1996,** *6,* 15–50.

[121] Bučko, T.; Hafner, J.; Lebègue, S.; Angyán, J. G. Improved description of the structure of molecular and layered crystals: Ab initio DFT calculations with van der Waals corrections, *J. Phys. Chem. A* **2010,** *114,* 11814–11824.

[122] Fishman, M.; Zhuang, H. L.; Mathew, K.; Dirschka, W.; Hennig, R. G. Accuracy of exchange-correlation functionals and effect of solvation on the surface energy of copper, *Phys. Rev. B* **2013,** *87,* 245402.

[123] Mathew, K.; Sundararaman, R.; Letchworth-Weaver, K.; Arias, T. A.; Hennig, R. G. Implicit solvation model for density-functional study of nanocrystal surfaces and reaction pathways, *J. Chem. Phys.* **2014,** *140,* 084106.

[124] Makov, G.; Payne, M. C. Periodic boundary conditions in ab initio calculations, *Phys. Rev. B* **1995,** *51,* 4014–4022.

[125] Hori, Y.; Murata, A.; Takahashi, R. Formation of hydrocarbons in the electrochemical reduction of carbon dioxide at a copper electrode in aqueous solution, *J. Chem. Soc., Faraday Trans. 1* **1989,** *85,* 2309–2326.

[126] Hussain, J.; Jónsson, H.; Skúlason, E. Calculations of product selectivity in electrochemical CO_2 reduction, *ACS Catal.* **2018,** *8,* 5240–5249.

[127] Wulff, G. Zur frage der geschwindigkeit des wachsthums und der auflösung der krystallflächen., *Z. Kristallog.* **1901,** *34,* 449–530.

[128] Carchini, G.; Almora-Barrios, N.; Revilla-López, G.; Bellarosa, L.; García-Muelas, R.; García-Melchor, M.; Pogodin, S.; Błoński, P.; López, N. How theoretical simulations can address the structure and activity of nanoparticles, *Top. Catal.* **2013,** *56,* 1262–1272.

[129] Reske, R.; Mistry, H.; Behafarid, F.; Roldan Cuenya, B.; Strasser, P. Particle size effects in the catalytic electroreduction of CO_2 on Cu nanoparticles, *J. Am. Chem. Soc.* **2014,** *136,* 6978–6986.

[130] Kortlever, R.; Shen, J.; Schouten, K. J. P.; Calle-Vallejo, F.; Koper, M. T. M. Catalysts and reaction pathways for the electrochemical reduction of carbon dioxide, *J. Phys. Chem. Lett.* **2015,** *6,* 4073–4082.

[131] Emsley, J. *Nature's building blocks: An A–Z guide to the elements;* Oxford University Press: 2011.

[132] *The New Encyclopaedia Britannica;* Encyclopaedia Britannica, Inc.: 1998.

[133] U.S. Department of the Interior, U.S Geological Survey, *Copper in November 2019*, `https://prd-wret.s3.us-west-2.amazonaws.com/assets/palladium/production/atoms/files/mis-201911-coppe.pdf`, 2020 Online; accessed 24 July 2020.

[134] Zhang, F.; Co, A. C. Direct evidence of local pH change and the role of alkali cation during CO_2 electroreduction in aqueous media, *Angew. Chem. Int. Ed.* **2020,** *59,* 1674–1681.

[135] Wang, X.; de Araújo, J. F.; Ju, W.; Bagger, A.; Schmies, H.; Kühl, S.; Rossmeisl, J.; Strasser, P. Mechanistic reaction pathways of enhanced ethylene yields during electroreduction of CO_2–CO co-feeds on Cu and Cu-tandem electrocatalysts, *Nat. Nanotechnol.* **2019,** *14,* 1063–1070.